Steel and Composite Structures, *Vol. 24, No. 6 (2017) 753-765*
DOI: https://doi.org/10.12989/scs.2017.24.6.753

Strength degradation of reinforced concrete piers wrapped with steel plates under local corrosion

Shengbin Gao [1,2], Jie Ni [3], Daxu Zhang [2] and Hanbin Ge [*4]

[1] *State Key Laboratory of Ocean Engineering, Shanghai Jiao Tong University, Shanghai, 200240, China*
[2] *Department of Civil Engineering, School of Naval Architecture, Ocean and Civil Engineering, Shanghai Jiao Tong University, Shanghai, 200240, China*
[3] *The IT Electronic 11th Design & Research Institute, Shanghai, 200233, China*
[4] *Department of Civil Engineering, Meijo University, Nagoya, 468-8502, Japan*

(*Received March 30, 2017, Revised May 07, 2017, Accepted May 28, 2017*)

Abstract. This paper aims to investigate the strength degradation of reinforced concrete piers wrapped with steel plates which corrode at the pier base by employing a three dimensional elasto-plastic finite element formulation. The prediction accuracy of the employed finite element analysis method is firstly verified by comparing the analytical results with test results. Then, a series of parametric studies is carried out to investigate the effects of steel plate's corrosion position along width direction, corrosion depth along plate thickness, corrosion range along width direction, and steel plate-concrete bonding degradation on the strength of the piers. It is observed that the strength degradation of the piers is closely related to steel plate's corrosion position, corrosion depth and corrosion range in the case of local corrosion on the webs. In contrast, when the base of flanges corrodes, the strength degradation of the piers is only related to steel plate's corrosion depth and corrosion range, and the influence of corrosion position on the strength degradation is very gentle. Furthermore, the strength of the piers decreases with the degradation of steel plate-concrete bonding behavior. Finally, the maximum strength of the piers obtained from numerical analysis corresponding to different bonding behavior is compared with theoretical results within an accepted error.

Keywords: bridge engineering; reinforced concrete pier; steel plate; local corrosion; steel plate-concrete bonding behavior; strength degradation

1. Introduction

Steel-concrete composite structures have obtained extensive applications in civil and building fields, which can make full use of strong tensile strength of steel and excellent compression strength of concrete. However, the weak ability for the steel to resist fire and corrosion is the main disadvantage of such composite structures. With respect to concrete-filled steel columns, extensive researches on seismic performance and fire resistance capacity have been carried out in the past few years. Susantha *et al*. (2001) presented a seismic design procedure for partially concrete-filled box-shaped steel columns by proposing a new failure criterion on the basis of the average strain of concrete and steel at critical regions. A uniaxial constitutive relation was developed to simulate the behavior of the filled-in confined concrete in steel columns. It was concluded that the inclusion of the confinement effects and softening behavior of concrete was important in the proposed prediction procedures. Fan *et al*. (2014) tested six three-dimensional joints between concrete-filled square steel tubular columns and composite steel-concrete beams to investigate the seismic performance of these composite joints under bidirectional reversal loads. The test specimens exhibited good strength and stiffness retention capacities and excellent energy dissipation. The influence of the bidirectional loading was significant when the joint was loaded into plastic range although it had minor effect in elastic range. Zhang *et al*. (2012) carried out experimental and analytical studies on the seismic behavior of steel I-beam to circular Concrete-Filled Steel Tubular (CFST) column assemblies with external diaphragms. Two exterior joints and two interior joints in a frame structure were tested and numerically simulated under constant axial loads on columns and cyclic vertical loads on beam ends. The results indicated that failure modes of the panels had significant effects on the stress distribution characteristic of the joints.

Fiber reinforced polymer (FRP) and steel plate are usually employed to strengthen reinforced concrete members. Dai *et al*. (2015) presented a three-dimensional finite element approach for the fire performance simulation of insulated FRP-strengthened RC beams. The proposed approach paid much attention to the constitutive modeling of concrete, steel, and FRP, as well as the bond-slip behavior of FRP-concrete and steel-concrete interfaces. Numerical results showed that the assumption of perfect bonding between FRP and concrete was liable to underestimate the beam deflections and thus predicted an unsafe fire resistance.

In the past few years, extensive researches have been carried out to investigate the effect of steel corrosion on the

*Corresponding author, Professor,
E-mail: gehanbin@meijo-u.ac.jp

ISSN: 1229-9367 (Print), 1598-6233 (Online)

behavior of steel structures and steel-concrete composite structures. Han *et al.* (2012) experimentally studied the performance of CFST members with square sections subjected to both loading and chloride corrosion. The main parameters considered were loading ratio and corrosion condition. The effects of both loading and corrosion on the behavior of CFST and reference hollow steel tubular members were analyzed on the basis of test results. Comparisons between the predicted ultimate strength by using the existing codes of DBJ/T13-51-2010 and EC4-2004 and the test results were proposed. Hou *et al.* (2013) investigated the failure modes and full-range behavior of the CFST stub columns and beams subjected to both loading and chloride corrosion. The mass loss at the external surface of steel tube caused by uniform corrosion was simulated through the "Model Change, Remove" elements. Simplified methods to calculate the strength of CFST stub column and beam under long-term loading and corrosion were illustrated on the basis of parameter analysis. Han *et al.* (2014) investigated the behavior of circular CFST stub columns under sustained load and chloride corrosion. A total of 17 specimens, including 11 stub CFST columns and 6 reference hollow steel tubes, were tested. It was found that corrosion could have significant influence on the ultimate strength of both CFST and hollow steel tubular stub columns. Parametric studies were carried out to study the main factors that influenced the residual axial strength of CFST stub columns under long-term loading and corrosion. Based on the parametric analysis, a simplified model for the residual axial strength ratio of CFST stub column was proposed. Hou *et al.* (2016) studied the flexural behavior of circular CFST beams under sustained load and chloride corrosion through both test and numerical analysis. It was found that corrosion caused noticeable deterioration to the flexural strength, while the ductility of CFST keeps well. A parametric study was carried out to find the main parameters that influenced the residual flexural strength. As a consequence, a simplified model was proposed to calculate the residual flexural strength of circular CFST under long-term load and corrosion.

Li *et al.* (2015) carried out test and numerical analysis to investigate the behavior of concrete-filled double skin steel tubular (CFDST) stub columns under preload, sustained load and chloride corrosion. A constant corrosion rate was assumed during the corrosion process. Ten layers of mesh were assigned for the corroded part of the outer tube, and the elements of each corroded layer were deactivated in each step to model the gradual thickness loss of the tube. It was found that the analytical results coincided well with the measured results in all loading stages. The corrosion of outer steel tube led to a large reduction of column strength, and the influences of the preload and long-term sustained load could be tentatively estimated by multiplying different coefficients. Sultana *et al.* (2015) employed the finite element analysis method to investigate the effect of random corrosion on the compressive strength capacity of marine structural units. A corrosion prediction model was incorporated to determine the thickness reduction with time. Corrosion-induced volume loss resulted in a greater reduction of ultimate strength for slender plates compared to stiffened panels, up to 45%, which showed that the structural element selection could strongly influence the accuracy of the estimated corrosion damage effect. Oszvald *et al.* (2016) presented a study on the remaining load-bearing capacity and the prospective behavior modes of corroded equal-leg angle-section members by test and numerical analysis. The corrosion was modelled by thickness reduction in the analysis. Compressive buckling tests and finite element analytical studies were carried out to analyze the modified buckling behavior and the ultimate strength. On the basis of the results, simplified design method was developed to predict the remaining compressive resistance.

With respect to the bonding strength degradation due to steel corrosion, Fang and Kou (2005) investigated the effect of steel corrosion on bonding strength in concrete structures by carrying out some axial loading tests on corroded stub columns. Sajedi and Huang (2015) proposed a simple probabilistic model of bonding strength considering corrosion using multi-variable regression based on a comprehensive database. The predictions were found to be accurate and unbiased when compared with the test results. The proposed bonding model was employed in the nonlinear finite element models of intact and corroded RC beams to investigate the importance of steel-concrete bond modeling on evaluating flexural behavior of the beams.

Cyclic behaviors of the corroded members and structures were also investigated. Kashani *et al.* (2014) employed an optical surface measurement technique to characterize three-dimensional corrosion pattern of reinforcing bars subjected to accelerated corrosion. The corroded bar specimens were tested under monotonic and cyclic axial loading. The optical measurement data were employed to develop a 3D micro-fiber finite element model for simulation of the physical testing and parametric study of the influence of corrosion pattern on stress–strain response of corroded bars. It was observed that the irregular cross sectional shape of pitted sections has a significant influence on the inelastic buckling and nonlinear cyclic response. Guo *et al.* (2015) carried out a cyclic test of coastal bridge piers considering the corrosion effects. Four test specimens, among which one was a sound structure and the others were structures with different levels of corrosion damage from accelerated corrosion, were used for the cyclic tests. The effects of the corrosion damage on the seismic behavior of the specimens were investigated based on the measured load - displacement hysteretic responses. The test results indicated that the seismic performance of the structure showed obvious degradation with the increase of corrosion level.

Up to date, the corrosion effect on the strength degradation of corroded steel bridge piers is very limited. Gao *et al.* (2016) employed a two-dimensional (2-D) elasto-plastic finite element formulation to investigate the load-carrying capacity degradation of reinforced concrete piers wrapped with steel plates due to occurrence of corrosion at the pier base. A series of parametric studies were carried out to investigate the effect of corrosion ratio and corrosion mode of steel plates located near the pier base on load-

carrying capacity of the piers. It was concluded that the load-carrying capacity of the piers decreased with the increase in corrosion ratio of steel plates. The degradation of load-carrying capacity resulted from the web's uneven corrosion mode was more serious than that under even corrosion mode, and the former case was more liable to occur than the latter case in actual engineering application. However, 2-D elasto-plastic finite element modelling of the piers cannot accurately account for the effect of local corrosion on flange and the bonding behavior degradation between steel plate and concrete on the strength of the piers. To overcome the above-mentioned disadvantages of 2-D modelling, three-dimensional (3-D) elasto-plastic finite element modelling is inevitably required.

This paper aims to investigate the strength degradation of reinforced concrete piers due to local corrosion of wrapped steel plates by employing an accurate 3-D elasto-plastic finite element formulation. First of all, the accuracy of the proposed finite element analysis method is verified by comparing the analytical results with test results and 2-D numerical results. After that, a series of parametric studies is carried out to investigate the effect of steel plate's corrosion position along width direction, corrosion depth along plate thickness, corrosion range along width direction, and the bonding degradation at the steel plate-concrete interface on the strength degradation of the piers. Lastly, the maximum strengths of the piers obtained from numerical analysis corresponding to different bonding behaviors are compared with the derived theoretical results within an accepted error.

2. Verification of 3-D finite element modelling

2.1 Finite element modelling of test specimens

Three reinforced concrete bridge piers with square section (600 × 600 mm) employed in Gao *et al*. (2016) are adopted here to verify the accuracy of the three-dimensional finite element modelling. Fig. 1(a) gives an original reinforced concrete pier (Case A). The piers designated as Case B and Case C in Figs. 1(b) and (c) respectively, are the piers wrapped with steel plates. The steel plates of Case B are fully fixed on the foundation, which is used to simulate an uncorroded pier. In contrast, in order to simulate the full corrosion state of the steel plates near the pier base, a 50 mm-height gap is set between the steel plate and the foundation in Case C. The test specimen is 3410 mm in height, and the steel plates are 1.6 mm in thickness. The elevation plan, cross section and the rebar assignment of the test specimen are given in Fig. 2.

3-D finite element analytical models of the test specimens are established by using ABAQUS software package (2010), as shown in Fig. 3. Eight-node isoparametric solid element (C3D8R) and four-node shell element with reduced integration technique (S4R) are employed to simulate concrete and steel plate, respectively. Truss element is used to model longitudinal rebars and stirrups, which are embedded in concrete elements. Contact elements are set between the steel plate and concrete to account for their interaction behaviors.

Material properties and uniaxial stress-strain curves of rebar, stirrup, steel plate and concrete are the same as those adopted in Gao *et al*. (2016), which are omitted here. It should be noted that the steel plate employed to strengthen the reinforced concrete piers in this paper is rather thin, which indicates that the confinement effect of steel plate on concrete cannot be expected so much. Therefore, the composite action between the steel tube and concrete is too weak to be accounted for here. Coulomb friction model is employed to simulate the friction behavior of contact element. It is assumed that a friction coefficient of 0.4 represents perfect bonding in the steel plate-concrete interface (Goto *et al*. 2010, Gao and Ge 2007). The degradation of bonding behavior for steel plate-concrete interface element is achieved by gradually adjusting the friction coefficient from 0.4 to 0.0 with an interval of 0.1.

With respect to the loading condition of the test specimen, a constant vertical load (550 kN) is uniformly applied first at the pier top. Then, an incremental lateral displacement is applied at the position which is 410 mm lower than the pier top, as shown in Fig. 2(a). In addition, the pier base is assumed to be fully fixed with the foundation.

2.2 Comparison of lateral load versus lateral displacement curves between test and analysis

Fig. 4 shows a comparison of lateral load versus lateral displacement curves between test and analysis. Both the

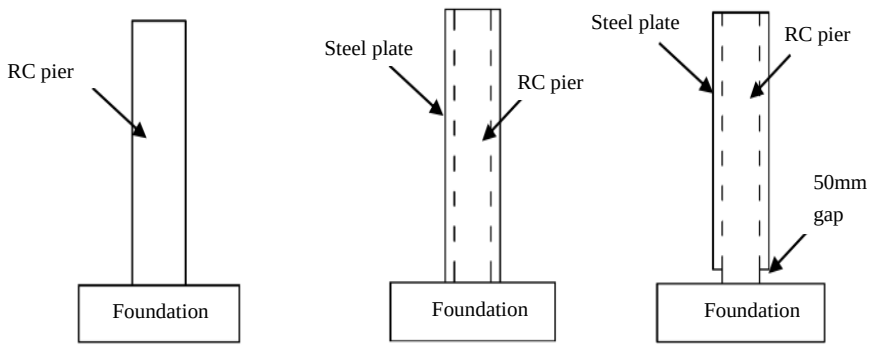

(a) Case A (b) Case B (c) Case C

Fig. 1 Sketch of test specimens

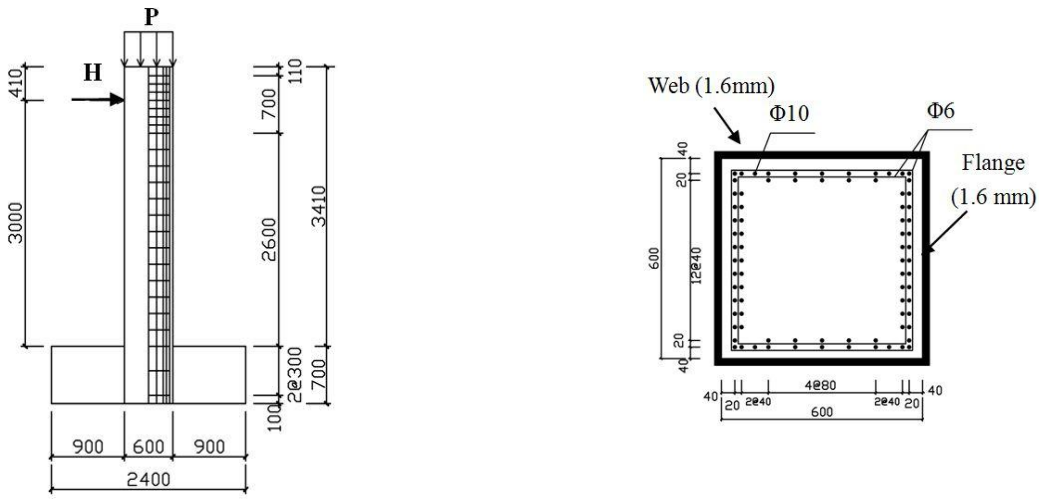

(a) Elevation plan (b) Cross section

Fig. 2 Geometry dimensions of test specimens

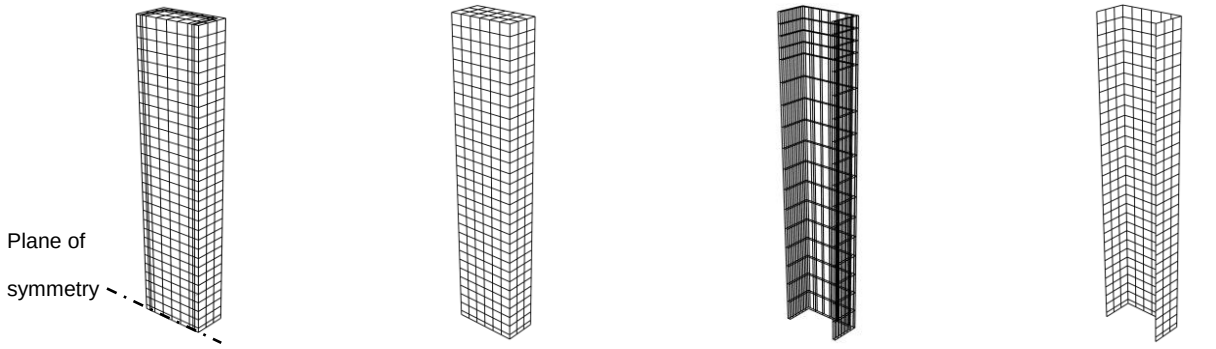

(a) Analytical model (b) Concrete (b) Rebar (d) Steel plate

Fig. 3 Finite element mesh of test specimen

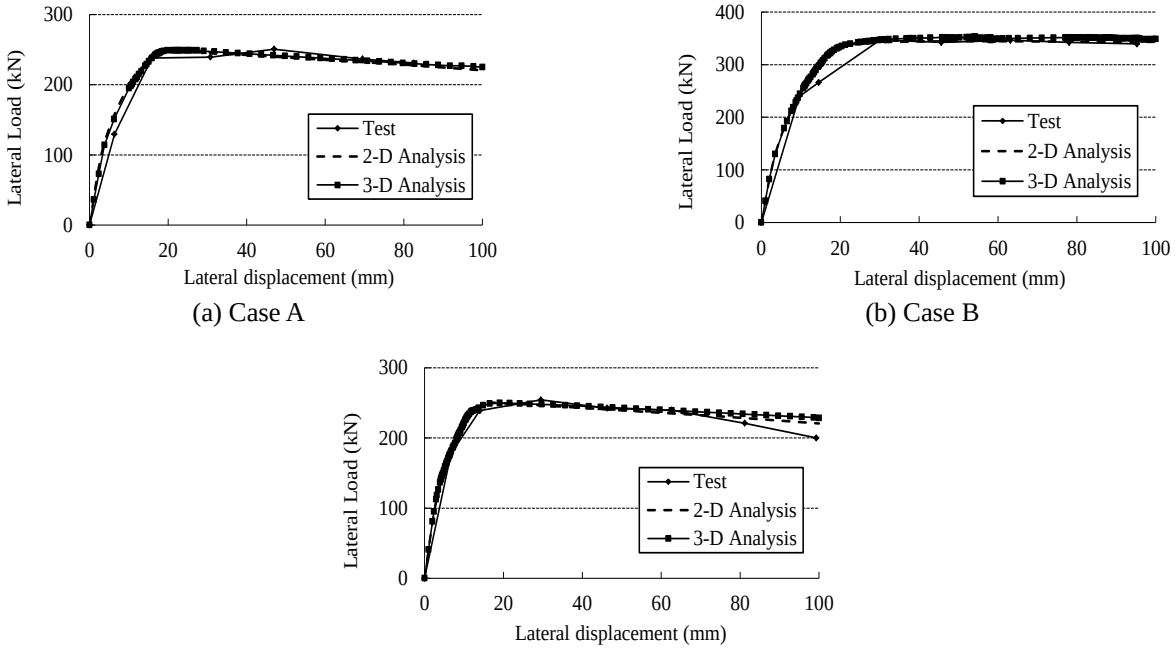

(a) Case A (b) Case B

(c) Case C

Fig. 4 Comparison of lateral load – lateral displacement curves between test and analysis

peak load and post-peak load obtained from 3-D numerical analysis are found to agree well with the test results. The strength of Case C decreases more rapidly in the test than that in the numerical simulation when the lateral displacement exceeds 70 mm. The possible reason lies in that the longitudinal rebar located in the compressive region near the pier base was found to buckle outwards in the test, which is not considered in the numerical analysis. As far as the corrosion state is concerned, Case B refers to an uncorroded pier, and Case C represents a fully corroded pier. It is observed from Figs. 4(a) and (b) that the maximum strength of Case B is about 100 kN larger than that of Case A, which means that wrapping steel plates outside the reinforced concrete pier can greatly improve the strength of the piers. The maximum strength of Case C is almost identical to that of Case A, which implies that the wrapped steel plate cannot improve the strength as soon as the steel plates near the pier base completely corrode.

Fig. 4 also compares lateral load versus lateral displacement curves obtained from 3-D analysis with that of 2-D analysis. It is found that the 3-D analytical results of three test specimens coincide well with the 2-D analytical results. As we had explained in Section 2.1, the confined effect of wrapped steel plates on the improvement of concrete compressive strength is not obvious because the thickness of steel plates (1.6 mm) is rather thinner than that employed in concrete-filled steel columns. Compared with 2-D analytical model, the main advantages of 3-D analytical model lie in that the local corrosion of steel plates and the bonding strength degradation of steel plate-concrete interface can be conveniently accounted for.

3. Local corrosion analysis of in-service pier

3.1 General introduction to in-service pier

The elevation plan, cross section and rebar assignment of an in-service pier (designated as P2 in the following description) is shown in Fig. 5. The cross section of pier P2 is 2800 mm (flange) × 3000 mm (web). The pier is 12400 mm in height, and the steel plate is 6 mm in thickness. A constant vertical load of 11090 kN is applied at the pier top, followed by an incremental lateral displacement. On the basis of Building Seismic Design Specification (2010) in China, the ultimate displacement is defined to be 1/50 of the pier height.

Fig. 6 gives a 3-D elasto-plastic finite element model of the specimen. The selection of element type and the analytical method are the same as those described in Section 2.1. The material properties of steel plate, rebar, and concrete are given in Table 1. It should be noted that the whole analytical model must be established in the case of local corrosion on flange.

3.2 Local corrosion analysis of in-service pier

As stated in Gao *et al*. (2016), corrosion distribution is very complex and irregular no matter along plate surface or along plate thickness. The steel plate-concrete bonding strength deteriorates due to adhesive aging or corrosion of steel plates. Therefore, some assumptions are adopted here to simplify the corrosion distribution and adhesive aging. Local corrosion of the piers is simulated by assuming different corrosion position and different plate thickness reduction. The steel plate-concrete bonding degradation is achieved by adjusting the friction coefficient of the contact elements.

In this section, a series of parametric studies is conducted to investigate the effect of steel plate's corrosion position along width direction, corrosion depth along plate thickness, corrosion range along width direction, and steel plate-concrete bonding degradation on the strength of the piers. The corroded range of steel plates is assumed to be 100 mm height from the pier base.

3.2.1 Effect of corrosion position

Table 2 lists the calculated cases corresponding to

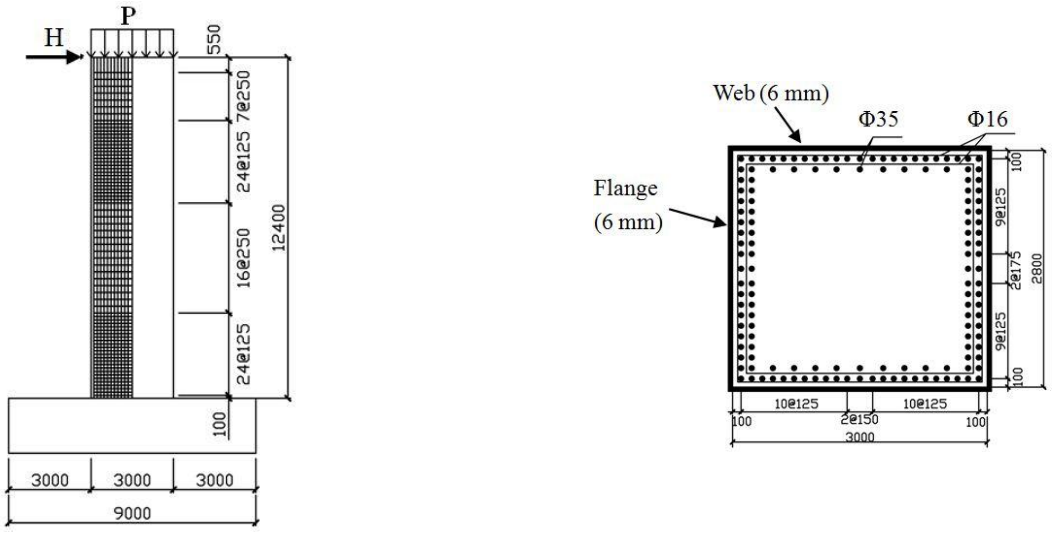

(a) Elevation plan (b) Cross section

Fig. 5 Geometry dimensions of in-service pier P2

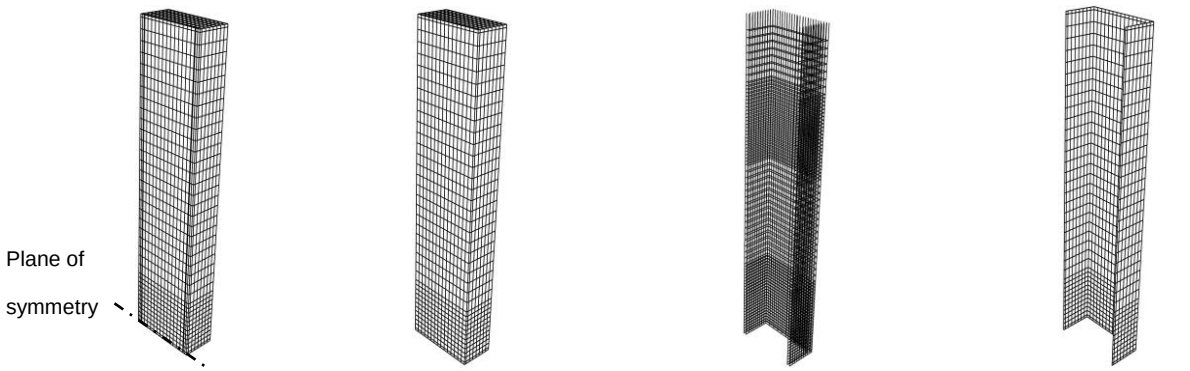

(a) Analytical model (b) Concrete (b) Rebar (d) Steel plate

Fig. 6 Finite element mesh of specimen F00W00

Table 1 Material properties

	Rebar		Stirrup		Steel plate		Concrete	
	Test	Pier P2	Test	Pier P2	Test	Pier P2	Test	Pier P2
Young's modulus (MPa)	2.06×10^5	2.06×10^5	2.06×10^5	2.06×10^5	2.06×10^5	2.06×10^5	2.78×10^4	2.78×10^4
Yield stress (MPa)	381	180	328	180	235	235	—	—
Tensile stress (MPa)	—	—	—	—	—	—	3.0	3.0
Compressive strength (MPa)	—	—	—	—	—	—	38.3	30.8

Table 2 Numerical results of the specimens corresponding to different corrosion position

Specimens	Maximum strength (kN)	Ultimate strength (kN)	Degradation ratio of maximum strength due to corrosion (%)	Degradation ratio of ultimate strength due to corrosion (%)
F00W00	6116	6004	—	—
F00W100-W1	5849	5616	4.4	6.5
F00W100-W2	5875	5714	3.9	4.8
F00W100-W3	5946	5809	2.8	3.2
F00W100-W4	6007	5867	1.8	2.3
F00W100-W5	5948	5850	2.7	2.6
F100W00-F1	5905	5745	3.4	4.3
F100W00-F2	5906	5747	3.4	4.3
F100W00-F3	5897	5742	3.6	4.4
F100W00-F4	5888	5751	3.7	4.2
F100W00-F5	5911	5752	3.3	4.2

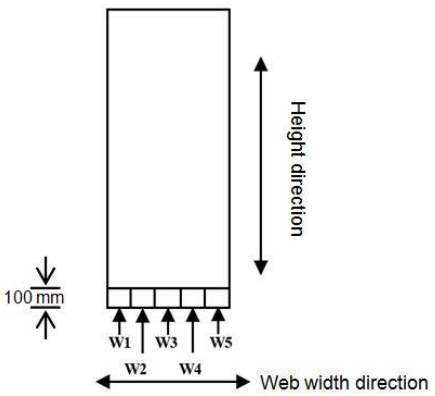

Fig. 7 Corrosion position of P2

different corrosion position. Here, taking "F00W100-W1" as an example to illustrate the naming rules of each specimen, "F" represents the tensile flange, and "W" stands for web. "00" followed by "F" means that there is no corrosion on flange, and "100" followed by "W" refers to full corrosion along web thickness. "W1" behind the hyphen refers to the corrosion position, as illustrated in Fig. 7. The corrosion range of each specimen is assumed to be 20% of the corresponding plate width. The naming rule with respect to the tensile flanges is similar to the webs.

Fig. 8 shows comparisons of lateral load - lateral displacement curves of the specimens corresponding to different corrosion position on web and tensile flange, respectively. It is observed from Fig. 8(a) that the corrosion position on web has a large effect on the strength. Fig. 9(a)

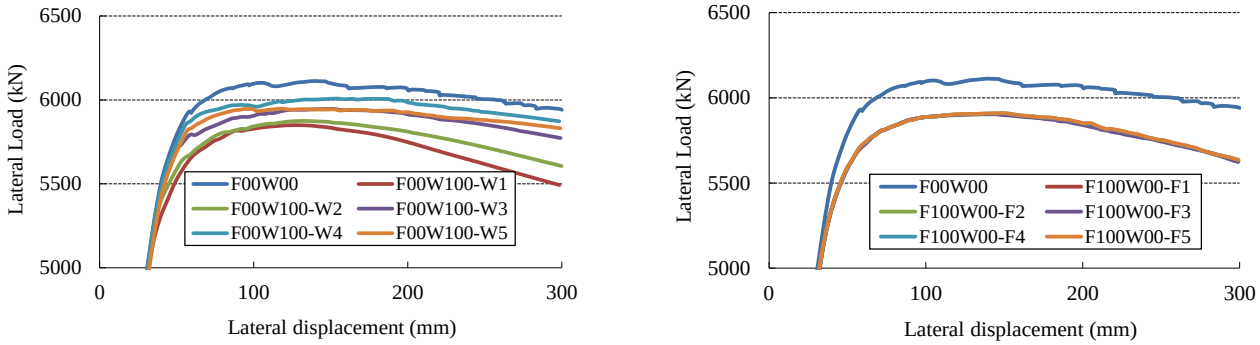

(a) Corrosion on web (b) Corrosion on flange

Fig. 8 Comparison of lateral load – lateral displacement curves (taking corrosion position as variant)

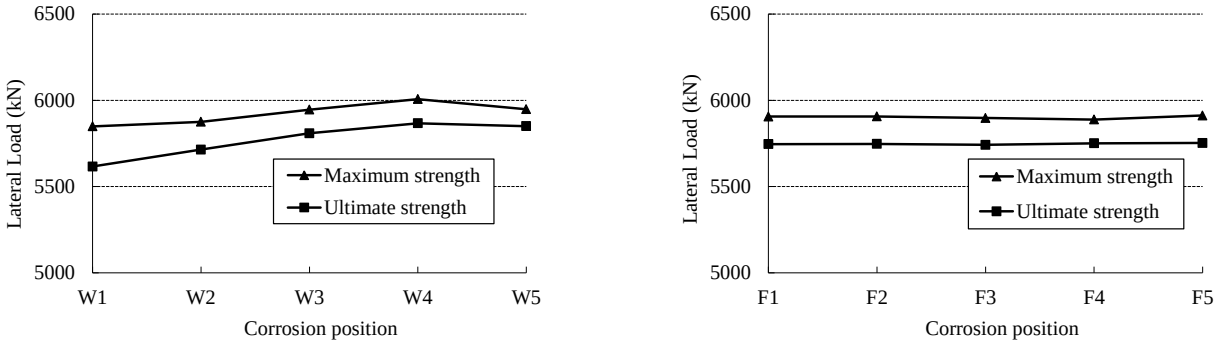

(a) Corrosion on web (b) Corrosion on flange

Fig. 9 Comparison of load-carrying capacity of the specimens (taking corrosion position as variant)

compares the strength of the specimens, in which the ultimate strength corresponds to the lateral displacement with 1/50 of the specimen height. It can be seen that the most affected specimen is F00W100-W1, the ultimate strength of which decreases by 6.5%. On the contrary, the least affected specimen is F00W100-W4. The reason that results in such substantial difference lies in that the web region near the tensile flange (W1) stays far away from the neutral axis, which contributes to the resistance of lateral load, to a large extent. The nearer to the neutral axis that the corroded web (W4) is, the less to resist the lateral load it is.

Fig. 8(b) gives the comparisons of lateral load - lateral displacement curves of the specimens with different corrosion position on tensile flange. An obvious strength degradation appears in the corroded specimens. Compared with the uncorroded specimen (F00W00), the maximum and ultimate strengths of the corroded specimen (F100W00-F1) decrease by 3.4% and 4.3%, respectively. As shown in Fig. 9(b), the effect of corrosion position on the strength is negligible in the case of flange corrosion.

3.2.2 Effect of corrosion depth along plate thickness

The effect of corrosion depth along plate thickness on the specimen's strength is investigated by assuming W1 region and F1 region to be locally corroded position,

Table 3 Numerical results of the specimens corresponding to different corrosion depth

Specimen	Maximum strength (kN)	Ultimate strength (kN)	Degradation ratio of maximum strength due to corrosion (%)	Degradation ratio of ultimate strength due to corrosion (%)
F00W00	6116	6004	—	—
F00W100-W1	5849	5616	4.4	6.5
F00W75-W1	5973	5781	2.3	3.7
F00W50-W1	6047	5897	1.1	1.8
F00W25-W1	6089	5965	0.4	0.6
F100W00-F1	5905	5745	3.4	4.3
F75W00-F1	5972	5874	2.4	2.2
F50W00-F1	6023	5900	1.5	1.7
F25W00-F1	6063	5955	0.9	0.8

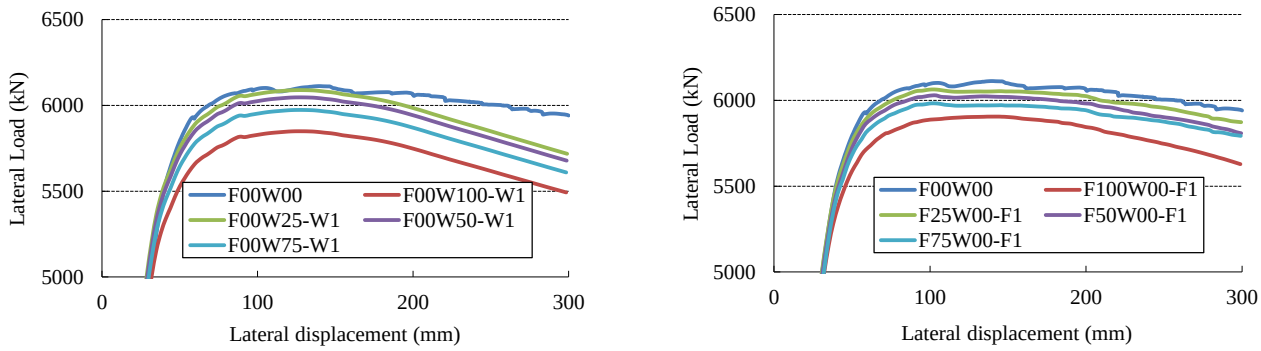

(a) Tensile web (W1) (b) Tensile flange (F1)

Fig. 10 Comparison of lateral load – lateral displacement curves (taking corrosion depth as variant)

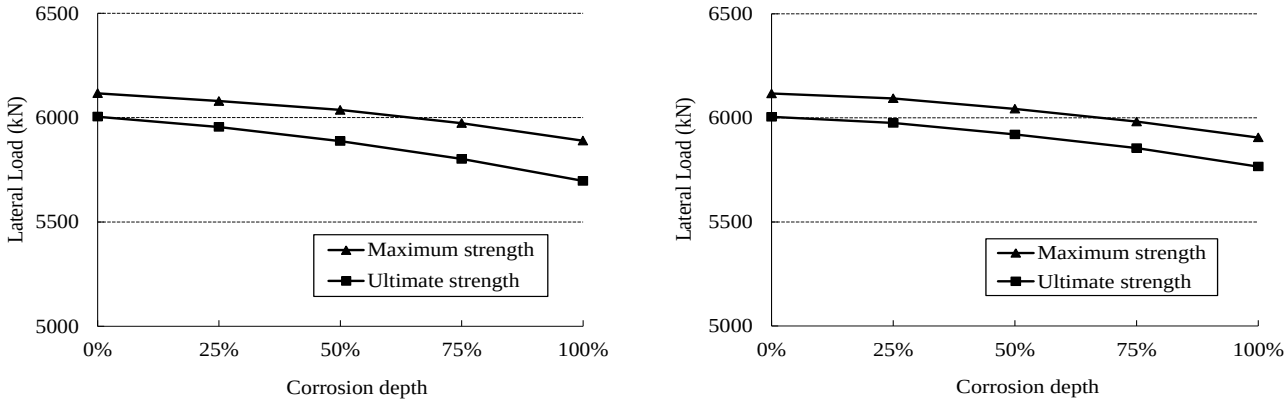

(a) Tensile web (W1) (b) Tensile flange (F1)

Fig. 11 Comparison of load-carrying capacity of the specimens (taking corrosion depth as variant)

Table 4 Numerical results of the specimens corresponding to different corrosion range

Specimen	Corrosion range (%)	Maximum strength (kN)	Ultimate strength (kN)	Degradation ratio of maximum strength due to corrosion (%)	Degradation ratio of ultimate strength due to corrosion (%)
F00W00	0	6116	6004	—	—
F00W100-W1	20	5849	5616	4.4	6.5
F00W100-W1-W2	40	5603	5332	8.4	11.2
F00W100-W1-W3	60	5406	5018	11.6	16.4
F00W100-W1-W4	80	5343	4949	12.6	17.6
F00W100-W1-W5	100	5283	4904	13.6	18.3
F100W00-F1	20	5905	5745	3.4	4.3
F100W00-F1-F2	40	5782	5513	5.5	8.2
F100W00-F1-F3	60	5571	5288	8.9	11.9
F100W00-F1-F4	80	5382	5048	12.0	15.9
F100W00-F1-F5	100	5172	4811	15.4	19.9

respectively. Table 3 lists the calculated cases with different corrosion depth along plate thickness. Fig. 10 shows comparisons of lateral load - lateral displacement curves of the specimens with different corrosion depth along web and flange thickness. The adjustment of corrosion depth is achieved by reducing the plate thickness in the local regions of W1 and F1, respectively. Fig. 11 compares the strengths of the specimens corresponding to different corrosion depth on tensile web and flange. It is observed that both the maximum and ultimate strengths decrease linearly as the increase in corrosion depth.

3.2.3 Effect of corrosion range

In order to investigate the effect of corrosion range at the web base on the strength of the piers, it is assumed that the corrosion begins from the web edge near the tensile

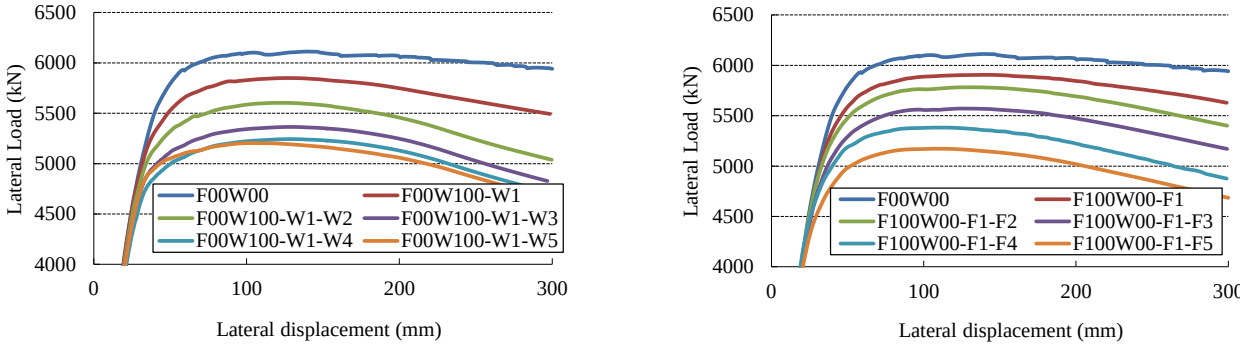

(a) Web (b) Flange

Fig. 12 Comparison of lateral load – lateral displacement curves (taking corrosion range as variant)

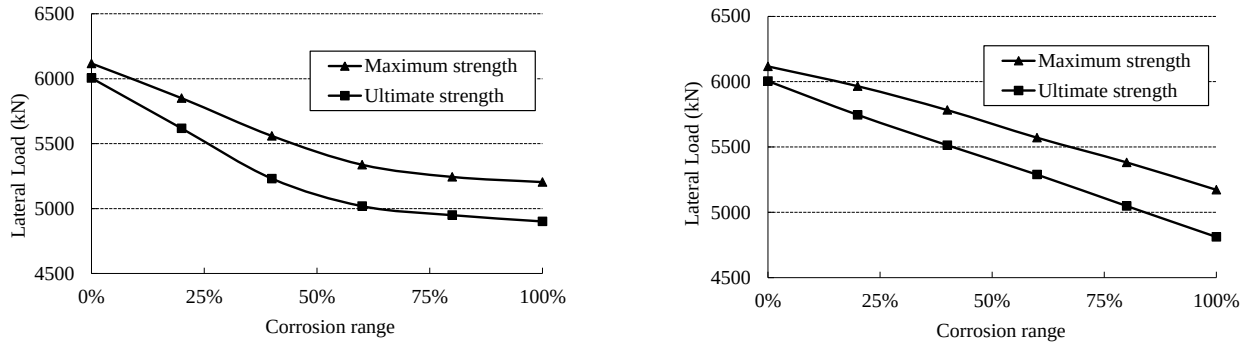

(a) Web (b) Flange

Fig. 13 Comparison of load-carrying capacity of the specimens (taking corrosion range as variant)

flange, and the corrosion range gradually propagates towards the compressive region as the corrosion ratio increases. In the case of flange corrosion, the corrosion takes place at the edge of tensile flange first, and then propagates till the whole tensile flange corrodes. Table 4 gives the lists of the calculated cases corresponding to different corrosion range. It should be noted that the corrosion depth is assumed to be 100% of steel plate thickness for both web and flange.

Fig. 12 shows the comparison of lateral load - lateral displacement curves corresponding to different corrosion range. It is observed that the maximum strength decreases as the corrosion range on both web and flange propagates. Comparisons of the specimen strength versus corrosion range are given in Fig. 13. It is observed from Fig. 13(a) that both the maximum and ultimate strengths decrease with the increase in corrosion range. However, the trend of strength degradation becomes gentle when the corrosion range is over 60% of the web width. A parabolic curve can be employed to describe the relationship between the strengths and corrosion range. The possible reason is that the web near the tensile flange is far away from the neutral axis, which can resist the lateral load, to a large extent. On the contrary, the tensile web near the neutral axis and the compressive web do not affect the strength so much. In the case of flange corrosion, both the maximum and ultimate strengths of the specimens decrease with the increase of corrosion range. There exists an obvious linear relationship between strength and corrosion range on flange.

3.2.4 Effect of steel plate-concrete bonding degradation

Five specimens (i.e., F00W00, F50W00-F1-F5, F100W00-F1-F5, F00W50-W1-W5, F00W100-W1-W5) are adopted here to investigate the effect of steel plate-concrete bonding degradation on the strength of the specimens. The bonding degradation is simulated by adjusting the friction coefficient of contact elements from 0.4 to 0.0. The friction coefficient of 0.4 refers to perfect bonding, while 0.0 indicates full loss of bonding behavior at the steel plate-concrete interface.

Fig. 14 shows the comparison of relative deformation between steel plate and concrete at the top of specimen F00W00 corresponding to different friction coefficient. It can be observed that the relative deformation becomes larger as the decrease of friction coefficient. Fig. 15 illustrates the neutral axis position shift of steel plate under different friction coefficient. In the case of friction coefficient with 0.4 (see Fig. 15(a)), the neutral axis shifts to the compressive region due to the interaction between steel plate and the inner concrete. However, when the friction coefficient decreases to zero (see Fig. 15(c)), the neutral axis of steel plate coincides with the center of cross section, which indicates that the steel plates work independently of the reinforced concrete pier.

Fig. 16 gives comparisons of lateral load - lateral displacement curves under different friction coefficient. To clarify the computed results more clearly, the lateral load on the ordinate axis begins from 4500 kN. It is seen that the

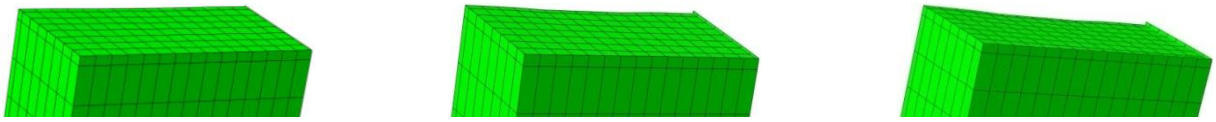

(a) μ = 0.4 (b) μ = 0.2 (c) μ = 0

Fig. 14 Comparison of relative deformation between steel plate and concrete at the top of Specimen F00W00 under different friction coefficient (Deformation scale = 1.0)

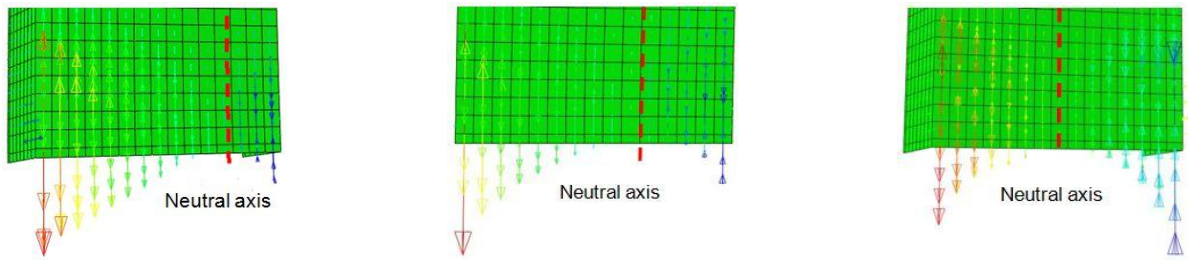

(a) μ = 0.4 (b) μ = 0.2 (c) μ = 0

Fig. 15 Comparison of the neutral axis shift under different friction coefficient

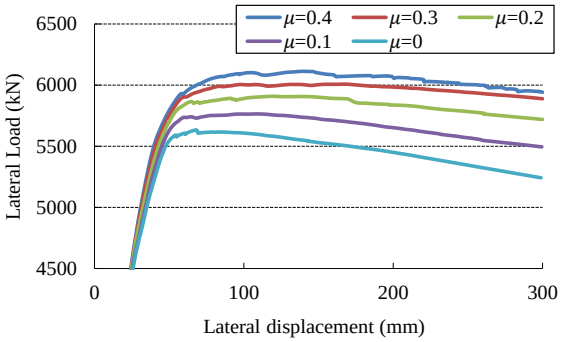

(a) F00W00

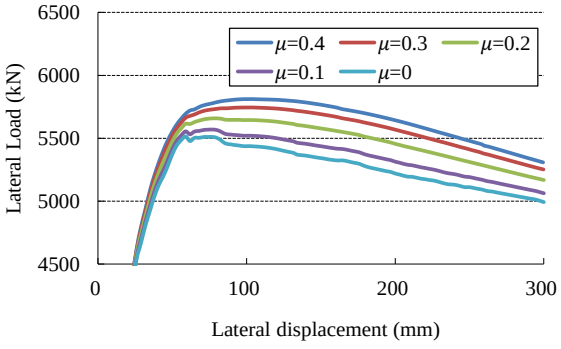

(b) F50W00-F1-F5

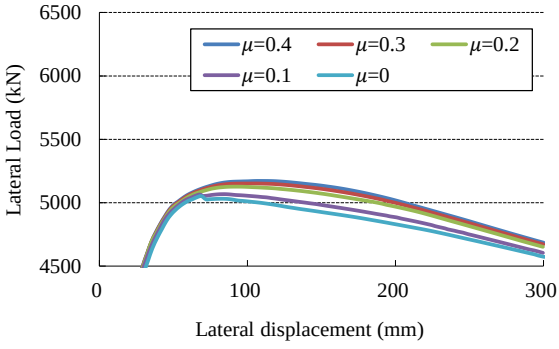

(c) F100W00-F1-F5

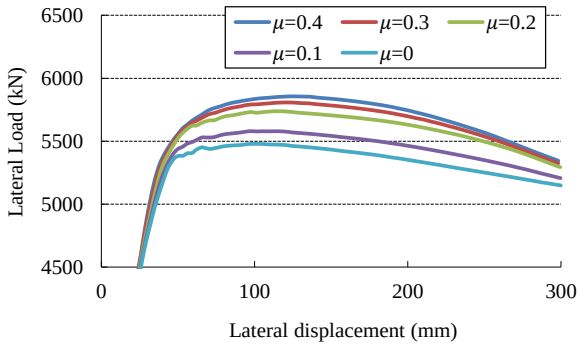

(d) F00W50-W1-W5

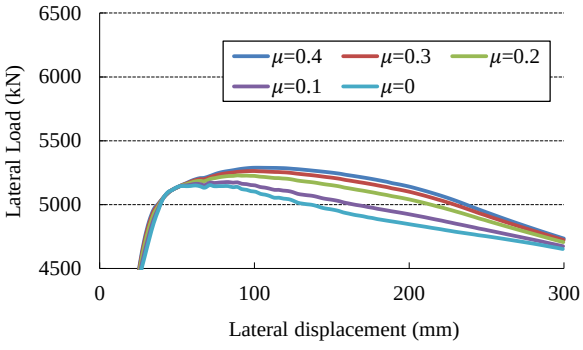

(e) F00W100-W1-W5

Fig. 16 Comparison of lateral load – lateral displacement curves under different friction coefficient

maximum strength of the specimens decreases as the bonding behavior becomes weak. Fig. 17 shows the variation of maximum strength corresponding to different friction coefficient. There exists a linear relationship between maximum strength and the friction coefficient. Besides, for the specimens without corrosion (see F00W00) or those with slight corrosion (see F00W50-W1-W5 and F50W00-F1-F5), the maximum strength decreases rapidly with the decrease of friction coefficient. However, in the case of severe corrosion (see F00W100-W1-W5 and F100W00-F1-F5), the friction coefficient has few effect on the maximum strength. The above phenomenon is understandable because the bonding behavior between the steel plate and concrete won't affect the maximum strengths if we assume a full corrosion at the pier base. When the steel plates at the pier base completely corrode, the wrapped steel plate cannot resist the lateral load any more, and the maximum strength in this case becomes just the same as that of the original reinforced concrete pier.

3.3 Theoretical verification of the analytical results

In order to verify the validity and accuracy of the analytical results, theoretical derivation is carried out to calculate the maximum strengths of the specimens F00W00, F100W00-F1-F5, and F00W100-W1-W5 corresponding to perfect bonding (i.e., u = 0.4) and full loss of bonding (i.e., u = 0.0), respectively. As shown in Fig. 15, the neutral axis shifts to the compressive region in the case of friction coefficient with 0.4. When the friction coefficient becomes zero, the neutral axis of steel plate coincides with cross section center, and the steel plates work independently of the reinforced concrete pier. It is assumed that the steel plate enters full plastic state when the specimen reaches maximum strength. In addition, the neutral axis position of the specimen with perfect bonding is determined by numerical analytical results. According to the force equilibrium condition between tensile force provided by steel plates and compressive force of concrete, the maximum strengths that the flange and web resist are given as follows.

(1) For a single web

$$H_{Web} = \frac{\sigma_y \cdot d_w \cdot b_w \cdot t_w}{2L} \tag{1}$$

(2) For a tensile flange

$$H_{Flange} = \frac{\sigma_y \cdot d_f \cdot b_f \cdot t_f}{L} \tag{2}$$

(3) For a compressive flange

$$H'_{Flange} = \frac{\sigma_y \cdot (b_w - d_f) \cdot b_f \cdot t_f}{L} \tag{3}$$

in which, σ_y is yield stress of steel plate, d_w is distance from web edge on tensile side to the neutral axis, d_f is distance from tensile flange to the neutral axis, t_w is web thickness, t_f is flange thickness, b_w is web width, b_f is flange width, L is specimen height. Table 5 compares the maximum strength obtained from theoretical calculation

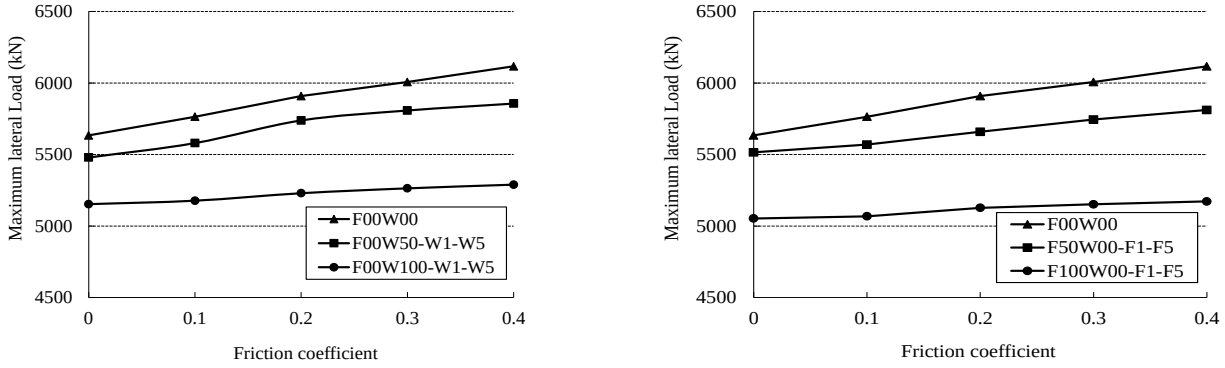

(a) Corrosion on Web (b) Corrosion on flange

Fig. 17 Effect of friction coefficient on maximum lateral load under different corrosion patterns

Table 5 Comparison of maximum strengths between FEM and theory

Specimen	Friction coefficient	Original pier (kN)	Flange (kN)	Web (kN)	Theoretical result (kN)	Numerical result (kN)	Error (%)
F00W00	0.4	3922	961	940	5823	6116	4.8
	0.0	3922	961	518	5401	5633	4.1
F100W00-F1-F5	0.4	3922	129	940	4991	5172	3.5
	0.0	3922	480	518	4920	5052	2.6
F00W100-W1-W5	0.4	3922	961	0	4883	5283	7.6
	0.0	3922	961	0	4883	5152	5.2

with numerical results. It can be seen that the numerical results are in general larger than the theoretical results, and the error between them is limited within 7.6%. The possible reason lies in that the yield stress is employed to calculate the maximum strength in the theoretical derivation, as shown in Eqs. (1)-(3). However, the steel plate has entered the strain hardening stage where the stress becomes larger than yield stress in the numerical analysis. In addition, as given in Eqs. (2)-(3), the distance from tensile flange to the neutral axis (d_f) can only be determined by conducting numerical analysis, which indicates that numerical simulation is inevitably required in evaluating the strength degradation of the corroded piers.

4. Conclusions

3-D elasto-plastic finite element formulation is employed to study the strength degradation of reinforced concrete piers wrapped with steel plates due to local corrosion at the pier base. A series of parametric studies is carried out to investigate the effects of steel plate's corrosion position along width direction, corrosion depth along plate thickness, corrosion range along width direction, and the steel plate-concrete bonding degradation on the strength of the piers. In addition, the maximum strengths of the piers obtained from numerical analysis corresponding to different bonding behavior are compared with the theoretical results. The main conclusions are summarized as follows.

(1) The lateral load - lateral displacement curves obtained from 3-D numerical analyses coincide well with the test results and 2-D numerical results, which indicate that the employed 3-D finite element formulation is accurate.
(2) The corrosion position along web width direction greatly affects the strength. The corroded steel plates staying far away from the neutral axis have a larger effect on the strength than those near the neutral axis. In contrast, the corroded position on the tensile flange has few effects on the strength of the piers.
(3) Both the maximum and ultimate strengths decrease linearly as the increase in corrosion depth on web and tensile flange.
(4) Both the maximum and ultimate strengths decrease with the increase of corrosion range on web and tensile flange. In the case of web corrosion, a parabolic curve between the strengths and corrosion range is observed. However, there exists a linear relationship between the strength and corrosion range in the case of flange corrosion.
(5) The maximum strengths of the specimens decrease as the bonding behavior deteriorates. The maximum strength of the specimens without corrosion or those with slight corrosion decreases more rapidly than those with severe corrosion as the coefficient friction is reduced.
(6) The maximum strength of the piers obtained from numerical analysis corresponding to different bonding behavior coincides with the theoretical results within an accepted error.

References

ABAQUS analysis user's manual (2010), SIMULIA, Providence, RI, USA.

Dai, J.G., Gao, W.Y. and Teng, J.G. (2015), "Finite element modeling of insulated FRP-strengthened RC beams exposed to fire", *J. Compos. Constr., ASCE*, **19**(2), 04014046(15).

Fan, J.S., Li, Q.W., Nie, J.G. and Zhou, H. (2014), "Experimental study on the seismic performance of 3d joints between concrete-filled square steel tubular columns and composite beams", *J. Struct. Eng., ASCE*, **140**(12), 04014094(13).

Fang, C.Q. and Kou, X.J. (2005), "The effect of steel corrosion on bond strength in concrete structures", *J. Shanghai Jiaotong Univ.* (*Sci.*), **E-10**(4), 436-440.

Gao, S.B. and Ge, H.B. (2007), "Numerical simulation of hollow and concrete-filled steel columns", *Adv. Steel Const., Int. J.*, **3**(3), 668-678.

Gao, S.B., Ikai, T., Ni, J. and Ge, H.B. (2016), "Load-carrying capacity degradation of reinforced concrete piers due to corrosion of wrapped steel plates", *Steel Compos. Struct., Int. J.*, **20**(1), 91-106.

GB50011-2010 (2010), Code for seismic design of buildings; China Architecture and Building Press, Beijing, China. [In Chinese]

Goto, Y., Kumar, G.P. and Kawanishi, N. (2010), "Nonlinear finite-element analysis for hysteretic behavior of thin-walled circular steel columns with in-filled concrete", *J. Struct. Eng., ASCE*, **136**(11), 1413-1422.

Han, L.H., Hou, C. and Wang, Q.L. (2012), "Square concrete filled steel tubular (CFST) members under loading and chloride corrosion: experiments", *J. Constr. Steel Res.*, **71**(1), 11-25.

Han, L.H., Hou, C.C. and Wang, Q.L. (2014), "Behavior of circular CFST stub columns under sustained load and chloride corrosion", *J. Constr. Steel Res.*, **103**(1), 23-36.

Hou, C., Han, L.H. and Zhao, X.L. (2013), "Full-range analysis on square CFST stub columns and beams under loading and chloride corrosion", *Thin-Wall. Struct.*, **68**, 50-64.

Hou, C.C., Han, L.H., Wang, Q.L. and Hou, C. (2016), "Flexural behavior of circular concrete filled steel tubes (CFST) under sustained load and chloride corrosion", *Thin-Wall. Struct.*, **107**, 182-196.

Kashani, M.M., Lowes, L.N., Crewe, A.J. and Alexander, N.A. (2014), "Finite element investigation of the influence of corrosion pattern on inelastic buckling and cyclic response of corroded reinforcing bars", *Eng. Struct.*, **75**, 113-125.

Li, W., Han, L.H. and Zhao, X.L. (2015), "Behavior of CFDST stub columns under preload, sustained load and chloride corrosion", *J. Constr. Steel Res.*, **107**, 12-23.

Oszvald, K., Tomka, P. and Dunai, L. (2016), "The remaining load-bearing capacity of corroded steel angle compression members", *J. Constr. Steel Res.*, **120**, 188-198.

Sajedi, S. and Huang, Q.D. (2015), "Probabilistic prediction model for average bond strength at steel-concrete interface considering corrosion effect", *Eng. Struct.*, **99**, 120-131.

Sultana, S., Wang, Y., Sobey, A.J., Wharton, J.A. and Shenoi, R.A. (2015), "Influence of corrosion on the ultimate compressive strength of steel plates and stiffened panels", *Thin-Wall. Struct.*, **96**, 95-104.

Susantha, K.A.S., Ge, H.B. and Usami, T. (2001), "A capacity prediction procedure for concrete-filled steel columns", *J. Earthq. Eng.*, **5**(4), 483-520.

Zhang, D.X., Gao, S.B. and Gong, J.H. (2012), "Seismic behaviour of steel beam to circular CFST column assemblies with external diaphragms", *J. Constr. Steel Res.*, **76**, 155-166.

BU